Numerical Study on Optimization of Active Layer Structures for GaN/AlGaN Multiple-Quantum-Well Laser Diodes

Jun-Rong Chen, Tsung-Shine Ko, Po-Yuan Su, Tien-Chang Lu, *Member, IEEE*, Hao-Chung Kuo, *Senior Member, IEEE*, Yen-Kuang Kuo, and Shing-Chung Wang, *Senior Member, IEEE, Fellow, OSA*

***Abstract*—Theoretical analysis for different active layer structures is performed to minimize the laser threshold current of the ultraviolet GaN/AlGaN multiple-quantum-well laser diodes by using advanced device simulation. The simulation results show that the lower threshold current can be obtained when the number of quantum wells is two or three and the aluminum composition in the barrier layer is about 10%–12%. This result is attributed to several different effects including electron leakage current, nonuniform carrier distribution, interface charge density induced by spontaneous and piezoelectric polarization, and optical confinement factor. These internal physical mechanisms are investigated by theoretical calculation to analyze the effects of quantum-well number and different aluminum compositions in barrier layer on laser threshold properties. Furthermore, the effect of quantum-well thickness is discussed as well. It is found that the optimal quantum-well thickness is about 3 nm due to the balance of the advantages of a large confinement factor against the disadvantages of significant quantum-confined Stark effect (QCSE).**

***Index Terms*—AlGaN, GaN, numerical simulation, semiconductor lasers, ultraviolet.**

I. Introduction

GROUP-III nitride semiconductors have received much attention in the past few years due to their promising applications in the field of optoelectronic devices such as light-emitting diodes (LEDs) used in solid-state lighting and laser diodes (LDs) used in high-density optical storage systems [1]–[3]. Recently, GaN-based high-efficiency optoelectronic devices in the blue and green regions have been realized and commercialized by achieving breakthroughs in the improvement of crystal quality and the realization of conductivity control [4], [5]. New ultraviolet laser diodes are also expected for the applications in frontier technologies such as super-high density optical storage systems, high-resolution laser printers, biological sensing, full-color projection displays, biotechnology applications, and an excitation source of optical catalyst [6], [7]. However, in the ultraviolet region, the high-efficiency group-III nitride optoelectronic devices are still difficult to fabricate, especially for ultraviolet laser diodes. One main reason is the difficulty in obtaining high-quality AlGaN materials due to the low diffusion length of aluminum atom or the aluminum-containing molecules on the surface of epitaxial film. Moreover, it is difficult to achieve high p-type conductivity in p-type AlGaN alloys due to high activation energy of Mg dopants [8]. A further problem is that the GaN/AlGaN system does not have isolation of carriers from nonradiative recombination centers unlike the InGaN/GaN system [7], [9]. Therefore, the reported lifetimes of ultraviolet laser diodes are still quite short from a commercial viewpoint.

Despite the material quality or fabrication problems, realizations of the ultraviolet laser diodes have been reported. 365-nm ultraviolet laser diodes using quaternary AlInGaN single-quantum-well structure were demonstrated under continuous wave (cw) operation at 25 °C by Masui *et al.* in 2003. The estimated lifetime of the 365 nm ultraviolet laser diodes was approximately 2000 h at an output power of 3 mW under cw operation at 30 °C [10]. Kneissl *et al.* also realized ultraviolet AlGaN multiple-quantum-well laser diodes with emission wavelengths between 359.7 and 361.6 nm in the same year [11]. Furthermore, Edmond *et al.* achieved cw laser diode operation from 348 to 410 nm by using AlInGaN/AlGaN material system grown on SiC substrates in 2004 [12]. Recently, GaN/AlGaN multiple-quantum-well ultraviolet laser diode with 350.9-nm-lasing wavelength has been demonstrated by Iida *et al.* [7], [13], [14]. Nevertheless, the laser diode was still operated under pulsed current injection.

In order to achieve high performance ultraviolet laser diodes, systematic and compact theoretical modeling is a necessary approach to improve existing laser structures and understand internal physical processes, which provides timely and efficient guidance toward the optimal structure design and device parameters. In this study, effects of quantum-well number and quantum-barrier aluminum composition on threshold properties

Manuscript received February 18, 2008; revised May 03, 2008. Current version published December 19, 2008. This work was supported in part by the MOE ATU program and in part by the National Science Council of the Republic of China under Contracts NSC 96-2221-E009-092-MY3, NSC 96-2221-E009-093-MY3, NSC 96-2221-E009-094-MY3, and NSC 96-2112-M-018-007-MY3.

J.-R. Chen, T.-S. Ko, P.-Y. Su, T.-C. Lu, H.-C. Kuo, and S.-C. Wang are with the Department of Photonics and the Institute of Electro-Optical Engineering, National Chiao Tung University, Hsinchu 30050, Taiwan, R.O.C. (e-mail: jrchen.eo95g@nctu.edu.tw; tsko.eo93g@nctu.edu.tw; tacashi128@gmail.com; timtclu@faculty.nctu.edu.tw; hckuo@faculty.nctu.edu.tw; scwang@cc.nctu.edu.tw).

Y.-K. Kuo is with the Department of Physics, National Changhua University of Education, Changhua 50058, Taiwan, R.O.C. (e-mail: ykuo@cc.ncue.edu.tw).

Digital Object Identifier 10.1109/JLT.2008.926939

of ultraviolet GaN/AlGaN multiple-quantum-well laser diodes are theoretically studied in detail by using an advanced LASer Technology Integrated Program (LASTIP), which self-consistently combines quantum well band structure calculations by $6\times 6k\cdot p$ theory, radiative and nonradiative carrier recombination, carrier drift and diffusion, and optical mode computation [15]. Since different quantum-barrier aluminum composition in GaN/AlGaN quantum wells result in different refractive indices, bandgap energies, and interface charge densities induced by spontaneous and piezoelectric polarization, it is expected that the laser performance will be varied with different quantum-barrier aluminum compositions. Although the similar research on AlGaN/AlGaN system has been reported by Chow *et al.* [16], we will focus our study on GaN/AlGaN system and systematically discuss the effects of quantum-well number, quantum-barrier aluminum composition, and quantum-well thickness on ultraviolet GaN/AlGaN multiple-quantum-well laser performance. Furthermore, how the different physical mechanisms influence the threshold properties is shown in this study as well.

II. Theoretical Model and Device Structure

The self-consistent LASTIP simulation program combines band structure and gain calculations with 2-D simulations of wave guiding, carrier transport and heat flux. The carrier transport model includes drift and diffusion of electrons and holes in devices. Built-in polarization induced by spontaneous and piezoelectric polarization is considered at hetero-interfaces of nitride related devices. In the quantum wells, self-consistent Poisson and Schrödinger equations are recomputed at every bias point for the states of quantum well levels and carrier distributions. In the optical mode model, a 2-D scalar complex wave equations is solved for the lateral modes. By calibrating with specific material parameters, LASTIP is a useful tool to access new designs, understand internal physical process, and optimize existing devices [17].

The physical model of the GaN/AlGaN quantum wells is considered in such a way that the conduction bands are assumed to be decoupled from valence subbands and have isotropic parabolic bands due to the larger bandgap of nitride semiconductor and the valence band structures, which includes the coupling of the heavy-hole (HH), the light-hole (LH), and the spin-orbit split-off bands, are calculated by the 6×6 Hamiltonian with envelop function approximation. By using the basis transformation, the 6×6 Hamiltonian can be transformed into a block-diagonalized Hamiltonian [18], [19]

$$H_{6\times 6}=\begin{bmatrix} H^U & 0 \\ 0 & H^L \end{bmatrix} \tag{1}$$

with

$$H^U=\begin{bmatrix} F & K_t & -iH_t \\ K_t & G & \Delta-iH_t \\ iH_t & \Delta+iH_t & \lambda \end{bmatrix} \tag{2}$$

$$H^L=\begin{bmatrix} F & K_t & iH_t \\ K_t & G & \Delta+iH_t \\ -iH_t & \Delta-iH_t & \lambda \end{bmatrix} \tag{3}$$

$$\begin{aligned} F&=\Delta_1+\Delta_2+\lambda+\theta \\ G&=\Delta_1-\Delta_2+\lambda+\theta \\ \lambda&=\frac{\hbar^2}{2m_0}(A_1k_z^2+A_2k_t^2)+\lambda_\varepsilon \\ \lambda_\varepsilon&=D_1\varepsilon_{\rm zz}+D_2(\varepsilon_{\rm xx}+\varepsilon_{\rm yy}) \\ \theta&=\frac{\hbar^2}{2m_0}(A_3k_z^2+A_4k_t^2)+\theta_\varepsilon \\ \theta_\varepsilon&=D_3\varepsilon_{\rm zz}+D_4(\varepsilon_{\rm xx}+\varepsilon_{\rm yy}) \\ K_t&=\frac{\hbar^2}{2m_0}A_5k_t^2 \\ H_t&=\frac{\hbar^2}{2m_0}A_6k_zk_t \\ \Delta&=\sqrt{2}\Delta_3,\ \text{and}\ k_t^2=k_x^2+k_y^2 \end{aligned} \tag{4}$$

where m_0 is the free electron mass. The A_i parameters are related to the hole effective masses. The crystal-field split energy is $\Delta_{\rm cr}=\Delta_1$ and the spin-orbit splitting is $\Delta_{\rm so}=3\Delta_2=3\Delta_3$. The D_i parameters are deformation potential constants.

To obtain the numerical parameters required for $k\cdot p$ calculations for the AlGaN materials, a linear interpolation between the parameters of the relevant binary semiconductors is utilized except for the unstrained bandgap energies. The material parameters of the binary semiconductors are taken from the paper by Vurgaftman and Meyer [20] and summarized in Table I. The unstrained AlGaN bandgap energies can be expressed as

$$\begin{aligned} E_{g,AlGaN}(x)&=x\cdot E_{g,AlN} \\ &\quad+(1-x)\cdot E_{g,GaN}-b\cdot x\cdot(1-x) \end{aligned} \tag{5}$$

where b is the bandgap bowing parameter of AlGaN, which is 0.7 eV in our calculation [20]. The temperature dependent bandgap energies of the relevant binary semiconductors are calculated using the commonly employed Varshni formula

$$E_g(T)=E_g(T=0)-\frac{\alpha T^2}{T+\beta}. \tag{6}$$

The values of α,β, and $E_g(T=0)$, i.e., the bandgap energy at zero Kelvin, of the binary alloys are listed in Table II [20]. The optical gain spectra of quantum-well structures, with the valence-band-mixing effect being taken into account, can be expressed by [21]

$$g(\hbar\omega)=g_{\rm sp}(\hbar\omega)\left[1-\exp\left(\frac{\hbar\omega-(F_c-F_v)}{k_BT}\right)\right] \tag{7}$$

$$\begin{aligned} g_{\rm sp}(\hbar\omega)&=\frac{2q^2\pi}{nc\varepsilon_0m_0^2\omega L_z} \\ &\quad\times\sum_{\sigma=U,L}\sum_{n,m}\int|M^\sigma_{\rm nm}(k_t)|^2 \\ &\quad\times\frac{f_n^c(1-f_{\sigma m}^v)(\gamma/\pi)}{(E_{\rm cn}-E_{\rm kpm}-\hbar\omega)^2+\gamma^2}\frac{k_t}{2\pi}dk_t \end{aligned} \tag{8}$$

where q is the free electron charge, h is the reduced Planck's constant, n is the index of refraction, ε_0 is the free-space dielectric constant, c is the speed of light, L_z is the thickness of

TABLE I
MATERIAL PARAMETERS OF THE BINARY SEMICONDUCTORS GAN, ALN, AND INN AT ROOM TEMPERATURE. ($\Delta_{cr} = \Delta_1, \Delta_{so} = 3\Delta_2 = 3\Delta_3$)

Parameter	Symbol (unit)	GaN	AlN
Lattice constant	a_0 (Å)	3.189	3.112
Spin–orbit split energy	Δ_{so} (eV)	0.017	0.019
Crystal–field split energy	Δ_{cr} (eV)	0.010	−0.169
Hole effective mass parameter	A_1	−7.21	−3.86
	A_2	−0.44	−0.25
	A_3	6.68	3.58
	A_4	−3.46	−1.32
	A_5	−3.40	−1.47
	A_6	−4.90	−1.64
Hydrost. deform. potential (c axis)	a_z (eV)	−4.9	−3.4
Hydrost. deform. potential (transverse)	a_t (eV)	−11.3	−11.8
Shear deform. potential	D_1 (eV)	−3.7	−17.1
	D_2 (eV)	4.5	7.9
	D_3 (eV)	8.2	8.8
	D_4 (eV)	−4.1	−3.9
Elastic stiffness constant	C_{33} (GPa)	398	373
Elastic stiffness constant	C_{13} (GPa)	106	108
Electron effective mass (c axis)	m_e^z/m_0	0.2	0.32
Electron effective mass (transverse)	m_e^t/m_0	0.2	0.30

TABLE II
VARSHNI PARAMETERS OF THE BINARY SEMICONDUCTORS GAN AND ALN

Parameter (unit)	GaN	AlN
α (meV/K)	0.909	1.799
β (K)	830	1462
$E_g(T=0)$ (eV)	3.51	6.25

quantum well, $h\omega$ is the photon energy, $M_{nm}(k_t)$ is the momentum matrix element in the quantum well, $1/\gamma$ is the intraband scattering relaxation time, E_{cn} is the nth conduction subband, E_{kpm} is the mth valence subband from the $k \cdot p$ calculation, f_c^n and f_v^m are the Fermi functions for the conduction band states and the valence band states, respectively. The indices n and m denote the electron states in the conduction band and the heavy hole (light hole) subband states in the valence band. To account for the broadening due to scattering, it is assumed that $\tau = 0.1$ ps [21]–[23] in the calculations. The conduction band offset ratio $\Delta E_c/\Delta E_g$ for the AlN/GaN interface is between 0.66 and 0.81 according to the recent calculations [24]. In our calculations, this value is assumed to be 0.7 based on published literatures [20].

The physical model of carrier transport is the traditional drift-diffusion model for semiconductors. The specific equations can be expressed as

$$\vec{J}_n = q\mu_n n \vec{F} + qD_n \nabla n \tag{9}$$

$$\vec{J}_p = q\mu_p p \vec{F} - qD_p \nabla p \tag{10}$$

TABLE III
NET SURFACE CHARGE DENSITY AT EACH INTERFACE OF THE GAN/ALGAN LASER DIODE

Interface	Built-in charge density
$GaN/Al_{0.18}Ga_{0.82}N$	-7.84×10^{12} cm^{-2}
$Al_{0.18}Ga_{0.82}N/Al_{0.08}Ga_{0.82}N$	$+4.56\times10^{12}$ cm^{-2}
$Al_{0.08}Ga_{0.92}N/Al_{0.25}Ga_{0.75}N$	-8.08×10^{12} cm^{-2}
$Al_{0.25}Ga_{0.75}N/Al_{0.08}Ga_{0.92}N$	$+8.08\times10^{12}$ cm^{-2}
$Al_{0.08}Ga_{0.92}N/GaN$	$+3.28\times10^{12}$ cm^{-2}
$GaN/Al_{0.08}Ga_{0.92}N$	-3.28×10^{12} cm^{-2}
$Al_{0.08}Ga_{0.92}N/Al_{0.18}Ga_{0.82}N$	-4.56×10^{12} cm^{-2}

TABLE IV
GAN MOBILITY PARAMETERS

Parameter (unit)	μ_{max} (cm^{2}V^{-1}s^{-1})	μ_{min} (cm^{2}V^{-1}s^{-1})	N_{ref} (cm^{-3})	α (–)
Electrons [33]	1405	80	0.778×10^{17}	0.71
Holes [32]	170	3	3×10^{17}	2

where n and p are the electron and hole concentrations, $\vec{J}_n$ and $\vec{J}_p$ are the current densities of electrons and holes, is the electrostatic field, μ_n and μ_p are the mobilities of electrons and holes. The diffusion constants D_n and D_p are replaced by mobilities using the Einstein relation $D = \mu k_B T/q$. The equations used to describe the semiconductor device behavior are Poisson's equation

$$\nabla \cdot (\varepsilon_0 \varepsilon \vec{F}) = q(p - n + p_D - n_A \pm N_f) \tag{11}$$

and the current continuity equations for electrons and holes

$$\frac{1}{q}\nabla \cdot \vec{J}_n - R_n + G_n = \frac{\partial n}{\partial t} \tag{12}$$

$$\frac{1}{q}\nabla \cdot \vec{J}_p + R_p - G_p = -\frac{\partial p}{\partial t} \tag{13}$$

where ε is the relative permittivity. G_n and R_n are the generation rates and recombination rates for electrons, G_p and R_p are the generation rates and recombination rates for holes, respectively. The electric field is affected by the charge distribution, including the electron and hole concentrations, dopant ions p_D and n_A, and other fixed charges N_f that are of special importance in nitride-based devices due to the effect of built-in polarization.

Built-in polarization induced due to spontaneous and piezoelectric polarization is known to influence the performance of nitride devices. In order to consider the built-in polarization within the interfaces of nitride devices, the method developed by Fiorentini *et al.* is employed to estimate the built-in polarization, which is represented by fixed interface charges at each hetero interface. They provided explicit rules to calculate the nonlinear polarization for nitride alloys of arbitrary composition [25]. For the GaN/AlGaN quantum-well lasers under study, the net surface charges at all interfaces are calculated and listed in Table III. Although the interface charges can be obtained by

TABLE V
LAYER STRUCTURE AND ROOM-TEMPERATURE PHYSICAL PARAMETERS OF THE GaN/AlGaN QUANTUM-WELL LASER UNDER STUDY (d, LAYER THICKNESS; $N_{\rm dop}$, DOPED CARRIER DENSITY; n, REFRACTIVE INDEX AT WAVELENGTH 355 NM). THE DOPED CARRIER DENSITY, $N_{\rm dop}$, REPRESENTS ACTUAL DENSITY OF FREE CARRIERS

Parameter (unit)	d (nm)	$N_{\rm dop}$ (1/cm^3)	n
p-GaN (contact layer)	20	1×10^{18}	2.9
p-$Al_{0.18}Ga_{0.82}N$ (cladding layer)	700	1.4×10^{17}	2.365
p-$Al_{0.08}Ga_{0.92}N$ (confining layer)	120	1×10^{17}	2.654
p-$Al_{0.25}Ga_{0.75}N$ (blocking layer)	20	1.4×10^{17}	2.167
i-$Al_{0.08}Ga_{0.92}N$ (barrier layer)	8	—	2.654
i-GaN (quantum well)	3	—	2.9
i-$Al_{0.08}Ga_{0.92}N$ (barrier layer)	8	—	2.654
i-GaN (quantum well)	3	—	2.9
i-$Al_{0.08}Ga_{0.92}N$ (barrier layer)	8	—	2.654
i-GaN (quantum well)	3	—	2.9
i-$Al_{0.08}Ga_{0.92}N$ (barrier layer)	8	—	2.654
n-$Al_{0.08}Ga_{0.92}N$ (confining layer)	120	1×10^{17}	2.654
n-$Al_{0.18}Ga_{0.82}N$ (cladding layer)	4000	2×10^{18}	2.365

this theoretical model, experimental investigations often find weaker built-in polarization than that predicted by theoretical calculation. It is mainly attributed to partial compensation of the built-in polarization by defect and interface charges [26]. Typical reported experimental values are of 20%, 50%, or 80% smaller than the theoretically calculated values [27]–[29]. As a result, 50% of the theoretical polarization values are used in our simulation from the average of the reported values.

A widely used empirical expression for modeling the mobility of electrons and holes is the Caughey–Thomas approximation, which is employed in our calculation and can be expressed as [30]

$$\mu(N) = \mu_{\min} + \frac{\mu_{\max} - \mu_{\min}}{1 + (N/N_{\rm ref})^{\alpha}} \tag{14}$$

where $\mu_{\min}$, $\mu_{\max}$, $N_{\rm ref}$, and α are fitting parameters according to the experimental mobility measurements. We employ this carrier mobility model for binary GaN material in our calculation. The relative parameters are summarized in Table IV [31], [32]. As for ternary AlGaN, the analytical expressions for mobility as a function of doping density have been established by Monte Carlo simulation for various nitride alloys [33]. Nonradiative recombination is commonly characterized by Shockley–Read–Hall (SRH) recombination and is governed by the defect-related nonradiative SRH lifetime ($\tau_{\rm SRH}$). Defect density and nonradiative lifetime depend on the substrate used and on the growth quality. In this study, we employ a common value of $\tau_{\rm SRH} = 1$ ns in our simulation [34]–[36]. The calculation of carrier capture and escape from the quantum wells is considered in accordance with the model provided by Romero *et al.* [37]. As for the parameter of refractive index, Adachi model is employed to calculate the refractive index values in each layer listed in Table V [38]–[40]. More description about the physical models utilized in LASTIP simulation program can be found in [41]–[43].

In this simulation, the GaN/AlGaN laser diode structure under study is referred to the real structures [7], [13], [14]. We first assume that the GaN/AlGaN laser diode is grown on an n-type $Al_{0.18}Ga_{0.82}$ N layer that is 4.0 μm in thickness. On top of this $Al_{0.18}Ga_{0.82}N$ layer is a 0.12-μm-thick n-type $Al_xGa_{1-x}N$ confining layer. The multiple-quantum-well active region consists of three 3-nm-thick GaN quantum wells and 8-nm-thick $Al_xGa_{1-x}N$ barriers. A 20-nm-thick p-type $Al_{0.25}Ga_{0.75}N$ electronic blocking layer is grown on top of the active region to reduce electron leakage into the p-type AlGaN layer [17], [44], [45]. Furthermore, a 0.12-μm-thick p-type $Al_xGa_{1-x}N$ confining layer and a 0.7-μm-thick p-type $Al_{0.18}Ga_{0.82}N$ cladding layer are grown. Finally, a 20-nm-thick p-type GaN cap layer is grown to complete the structure. The aluminum composition in the $Al_xGa_{1-x}N$ barrier and the confining layers are varied from 8% to 16%. The effective active region of the ridge geometry is 4 μm in width and the cavity is 500 μm in length. The reflectivities of the two end mirrors are set at 50% and 90%, respectively. The doping concentrations in each layer and the detailed device structure are described in Table V. The doping data in this table give the actual densities of free carriers.

III. SIMULATION RESULTS AND DISCUSSION

The laser output power of the GaN/$Al_{0.08}Ga_{0.92}N$ laser diode structure as a function of input current is shown in Fig. 1 when the number of quantum wells varies from one to five. The simulation results indicate that the best laser performance is obtained when the number of quantum wells is three and the worst laser performance is observed when the number of quantum wells is one. In order to further study the effects of quantum-barrier aluminum composition on threshold current of the GaN/$Al_xGa_{1-x}N$ laser diodes. The threshold current values of the laser diodes with different barrier aluminum compositions are plotted in Fig. 2 when the number

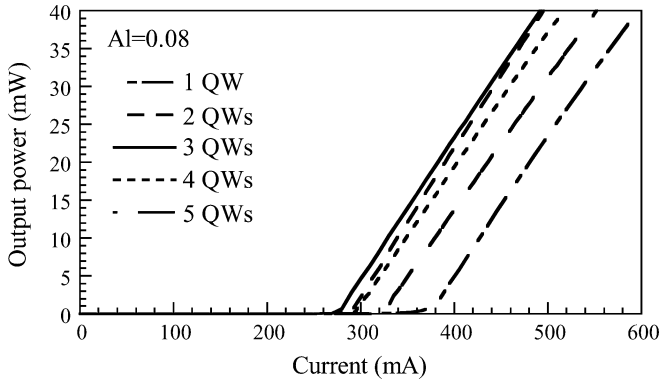

Fig. 1. Laser output power of the GaN/$Al_{0.08}Ga_{0.92}N$ laser diode structure as a function of input current when the number of quantum wells varies from one to five.

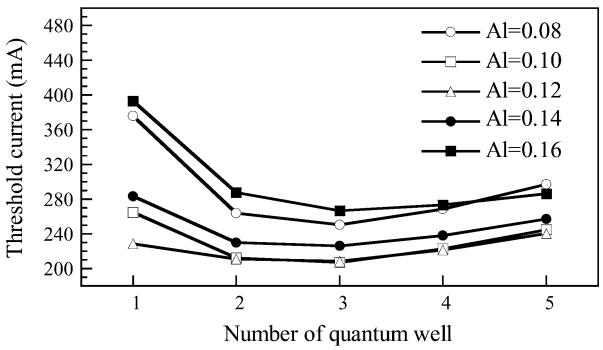

Fig. 2. Threshold current values of laser diodes with different barrier aluminum composition when the number of quantum well varies form one to five. The quantum-well thickness is 3 nm.

of quantum wells varies form one to five. According to the simulation results, optimal barrier aluminum composition is about 10%–12% for the GaN/$Al_xGa_{1-x}N$ quantum-well lasers. Lower and higher aluminum compositions in $Al_xGa_{1-x}N$ barrier/confining layer result in larger threshold current values. Furthermore, in this study the optimized number of quantum wells for GaN/$Al_xGa_{1-x}N$ laser diodes is found to be three. This optimal quantum-well number consists with that of the experimental laser structure employed by Iida *et al.* [7], [13], [14]. All possible internal physical mechanisms which lead to these results will be discussed and analyzed in detail in the following content.

A. Electron Leakage Current

In order to understand the internal physical mechanisms which result in the worst laser performance in the cases of lower barrier aluminum composition and fewer number of quantum wells, the vertical electron current density profiles within the active regions of laser structures with $Al_{0.08}Ga_{0.92}N$ and $Al_{0.16}Ga_{0.84}N$ barrier layers, respectively, are plotted in Fig. 3 at 500-mA injection current. This driving current is chosen to be above the threshold current values of the laser diodes under study. The positions of five quantum wells are marked with gray areas. The left-hand side of the figure is the n-side of the device. The electron current is injected from n-type layers into quantum wells and recombines with holes

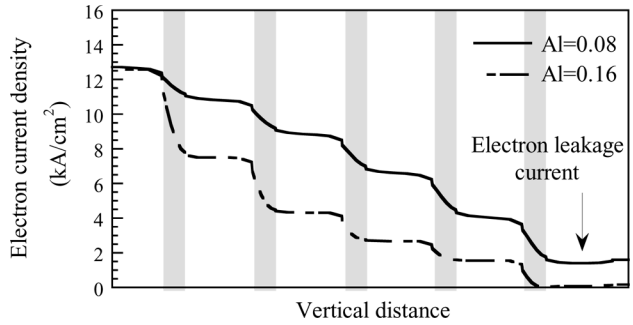

Fig. 3. Vertical electron current density profiles within the active regions of laser structures with $Al_{0.08}Ga_{0.92}N$ and $Al_{0.16}Ga_{0.84}N$ barrier layers at 500-mA injection current.

in quantum wells. Therefore, the electron current density is reduced in the quantum wells. Electron current which overflows through quantum wells is viewed as leakage current. The problem of electron leakage current plays an important role for the optical performance of III-nitride laser diodes which are mostly operated at high injection level [17], [44], [45]. Several methods have been proposed to suppress the leakage current, such as increasing p-type doping concentration to increase the barrier height [46] and employing the multi-quantum barrier (MQB) structure to block the overflowing electrons [47]. Besides, optimizing the active region structure is another approach to minimize the electron leakage current. The increases of quantum-well number and height of quantum barrier provide better electron confinement, especially for high operation temperature and high current injection. In Fig. 3, the electron leakage current is still observed even though the number of quantum wells is five in the GaN/$Al_{0.08}Ga_{0.92}N$ laser diode structure. On the contrary, when the barrier aluminum composition increases from 8% to 16%, better electron confinement is provided and electron leakage current is hardly observed. Therefore, the increase in barrier height by adding more aluminum composition in barrier layer is also an effective approach to suppress the electron leakage current except for the increase in quantum-well number.

B. Nonuniform Carrier Distribution

Multiple-quantum-well laser diode performance is significantly affected by nonuniform carrier distribution within the multiple-quantum-well active regions [48]. It is expected that this effect will be more critical for nitride-based laser diodes since the conduction band offset is relatively higher than that of conventional III-V semiconductor heterostructures [49]. The nonuniform carrier distribution will also lead to the nonuniform interband gains within multiple-quantum-well active regions. In order to study the effect of nonuniform carrier distribution induced by quantum-well number and quantum-barrier aluminum composition, the interband gains in the active regions of the GaN/$Al_xGa_{1-x}N$ laser diodes with different barrier aluminum compositions are illustrated in Fig. 4 at an input current of 500 mA when the number of quantum wells varies from one to five. In Fig. 4(a), the GaN/$Al_{0.08}Ga_{0.92}N$ laser diode structure induces serious electron leakage current due to poor electron confinement, which results in lower interband

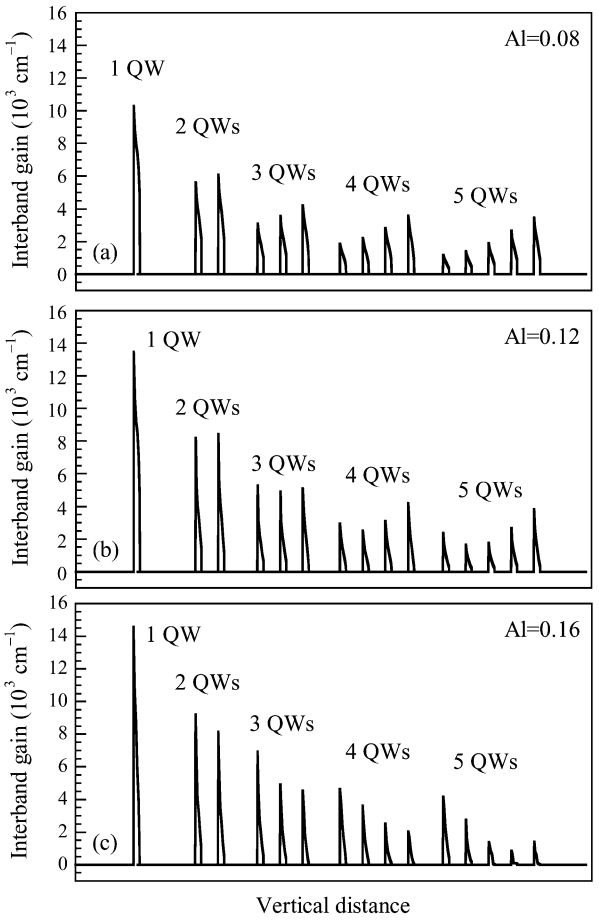

Fig. 4. Interband gain in the active region of the GaN/AlGaN laser diodes with a $Al_xGa_{1-x}N$ barrier of (a) $x = 0.08$, (b) $x = 0.12$, and (c) $x = 0.16$ at an input current of 500 mA when the number of quantum wells varies from one to five.

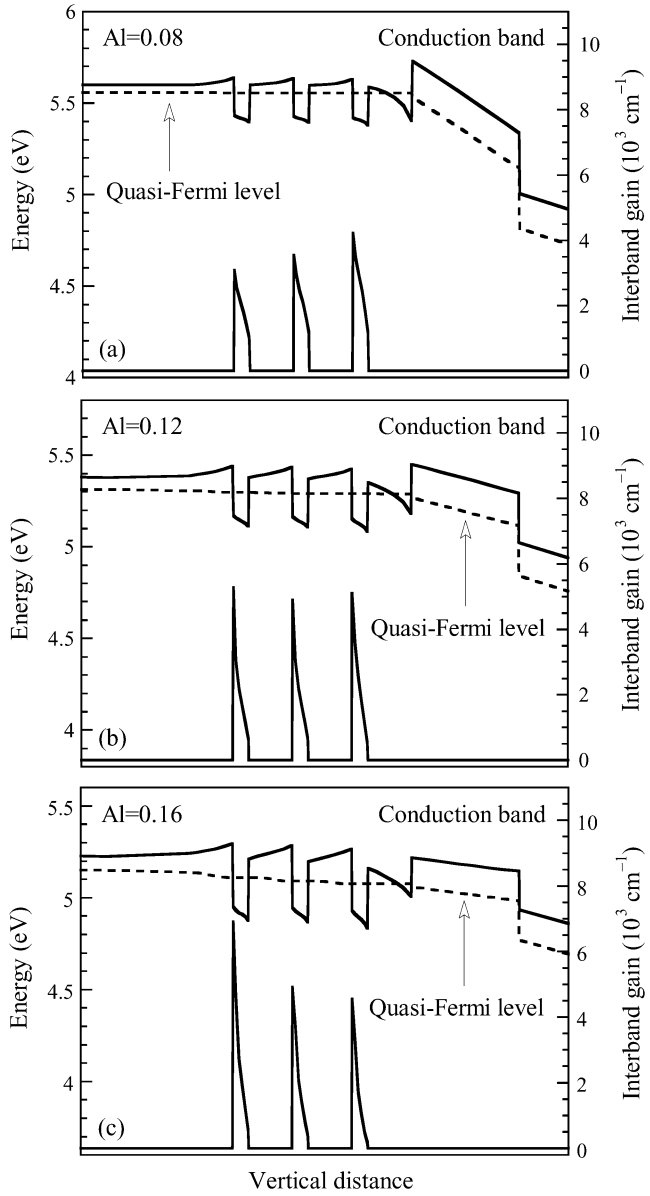

Fig. 5. Conduction band structure, quasi-Fermi level, and interband gain for the three-quantum-well active layers with a $Al_xGa_{1-x}N$ barrier of (a) $x = 0.08$, (b) $x = 0.12$, and (c) $x = 0.16$ at an input current of 500 mA.

gain, especially for the laser structures with fewer number of quantum wells. Therefore, when the number of quantum wells is less than three, the interband gain increases with aluminum composition in barrier layer. However, as shown in Fig. 4(c), although the GaN/$Al_{0.16}Ga_{0.92}N$ laser diode structure provides better carrier confinement due to the higher aluminum composition in barrier layer, the interband gain values in the quantum wells become very nonuniform, and the highest interband gain is always observed in the well closest to the n-side. Furthermore, relatively more uniform interband gain values in multiple-quantum-well active region are observed when the barrier aluminum composition is 0.12, as shown in Fig. 4(b). Consequently, when the number of quantum wells is more than three, the nonuniform interband gain in multiple-quantum-well active region is obvious with increasing aluminum composition in barrier layer.

The deep quantum well with a high aluminum composition barrier is the main mechanism which makes the nonuniform interband gain in active region with multiple-quantum-well structure. To further understand the effects of nonuniform interband gain on laser threshold current, Fig. 5 shows the conduction band structure, quasi-Fermi level, and interband gain for the three-quantum-well active layers with a $Al_xGa_{1-x}N$ barrier of (a) $x = 0.08$, (b) $x = 0.12$, and (c) $x = 0.16$ under an operation current of 500 mA. In Fig. 5(a), shallow quantum wells make the electron overflow severe, which can be observed from the distribution of quasi-Fermi level across the three quantum wells. Nevertheless, as the aluminum composition in barrier layer increases, the nonuniform distribution of electron carriers in the deep quantum wells is obvious, as indicated in Fig. 5(c). In this situation, the interband gain decreases gradually as the well position is close to the p-type layer. Consequently, by comparing Fig. 5(a), (b), and (c), when altering the aluminum composition of the barrier layers, a compromise between reducing the electron overflow and an uniform electron distribution is required. Hence, the results for triple-quantum-well GaN/$Al_xGa_{1-x}N$ active layer structure with $x = 0.12$ gives the optimum performance.

C. Spontaneous and Piezoelectric Polarization

Fig. 6 shows the electron and hole concentration distribution in active region for the laser structures with a $Al_xGa_{1-x}N$ barrier of (a) $x = 0.08$, (b) $x = 0.12$, and (c) $x = 0.16$ under an operation current of 500 mA. In addition to the effects of barrier height on the electron overflow and the nonuniform electron distribution, it is noteworthy that the energy barrier height created by $Al_{0.25}Ga_{0.75}N$ electronic blocking layer is substantially reduced by the high density of positive polarization charges at the interface between the $Al_xGa_{1-x}N$ barrier layer and the $Al_{0.25}Ga_{0.75}N$ electronic blocking layer, as indicated in Table III and Fig. 5. This condition is more obvious for laser diode with $Al_{0.08}Ga_{0.92}N$ barrier. Under this condition, the electrons are attracted by Coulomb force and accumulate at this interface, which leads to strong band bending, as shown in Figs. 5(a) and 7(a). Consequently, the increase of laser threshold current will be expected due to the enhanced electron carrier leakage from active layer to p-type layer [46]. Moreover, the high density of positive polarization charges inhibits the injection of hole carriers into quantum wells. As for the injected holes in quantum wells, they will be attracted by the high density of electrons accumulated at this interface. Because of these two mechanisms, hole concentration decreases from p-side quantum well to n-side quantum well gradually, which leads to the same trend for quantum-well interband gain, as evident in Figs. 4(a), 5(a), and 6(a). In the case of the laser diode with $Al_{0.16}Ga_{0.84}N$ barrier, the density of positive polarization charges at this interface is relatively lower, which leads to lower electron accumulation at the interface between the $Al_{0.16}Ga_{0.84}N$ barrier layer and the $Al_{0.25}Ga_{0.75}N$ electronic blocking layer, as shown in Figs. 5(c) and 6(c). Therefore, the injection of hole carriers is easier than that of laser diode with $Al_{0.08}Ga_{0.92}N$ barrier. Furthermore, the injected holes in quantum wells are attracted by the accumulated electrons in the n-side quantum well, which results from the deeper well due to the higher aluminum composition in barrier layer. For these two reasons, hole concentration increases from p-side quantum well to n-side quantum well gradually, which leads to the same trend for quantum-well interband gain, as evident in Figs. 4(c), 5(c), and 6(c).

Fig. 7 depicts the percentage of electronic leakage current as a function of the bias current for the laser diodes with three-quantum-well active layers with a $Al_xGa_{1-x}N$ barrier of $x = 0.08$, $x = 0.12$, and $x = 0.16$, respectively. The percentage of electron leakage current is defined as the ratio of the electron current overflowed to the p-type layer to that injected into the active region of the laser diodes. The percentage of electron leakage current increases with increasing input current and decreasing aluminum composition in barrier layers. When the input current is below the threshold current values, which are about 200–250 mA, the leakage current rises obviously with input current. Nevertheless, when the input current is larger than the threshold current, the mechanism of stimulated emission occurs, which results in significant carrier recombination in quantum wells. Consequently, the increase of leakage current is suppressed as the input current is above the threshold current. Furthermore, the increase of the electron leakage current of the laser diode with $Al_{0.08}Ga_{0.92}N$ barrier layer is more obvious with the increasing input current as compared with that of the laser diode with $Al_{0.16}Ga_{0.84}N$ barrier layer. This result is attributed to the above reasons, such as barrier height and electron accumulation at the interface of barrier layer and electronic blocking layer. Fig. 8 shows 50% of the theoretically calculated interface charge densities at

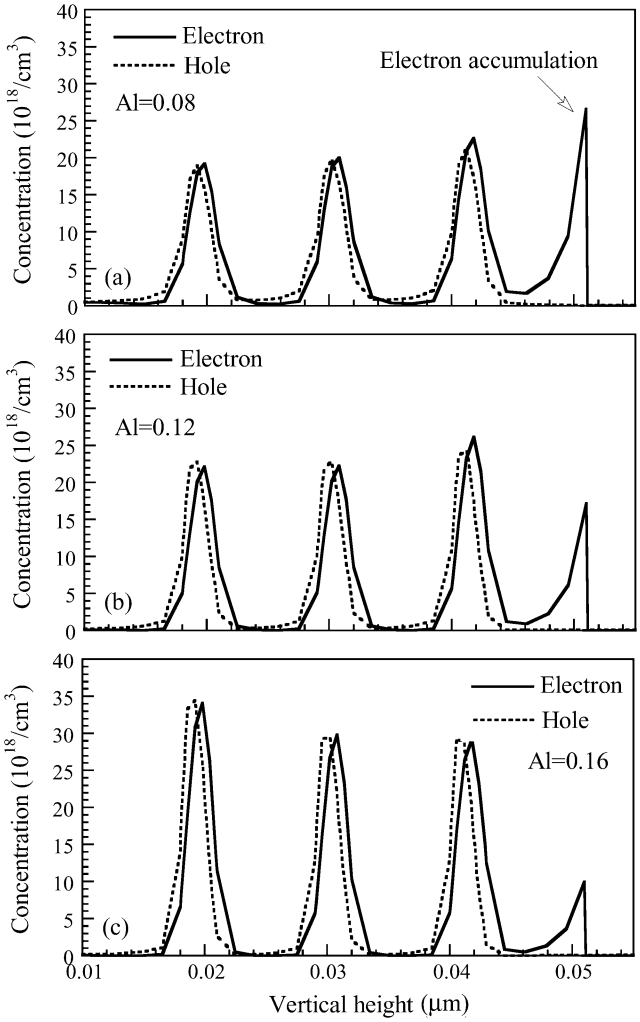

Fig. 6. Electron and hole concentration distribution in active region for the laser structures with a $Al_xGa_{1-x}N$ barrier of (a) $x = 0.08$, (b) $x = 0.12$, and (c)$x = 0.16$ under an operation current of 500 mA.

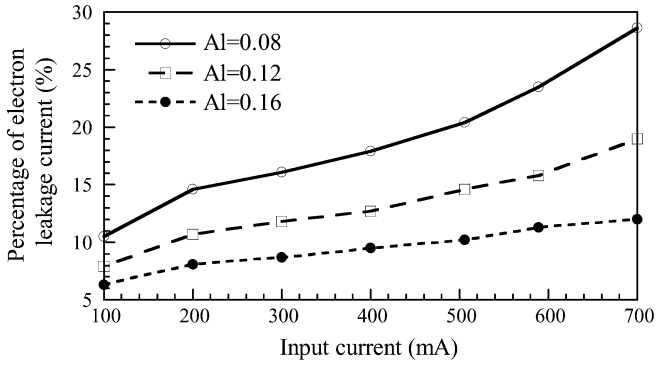

Fig. 7. Percentage of electronic leakage current as a function of the bias current for the laser diodes with three-quantum-well active layers with a $Al_xGa_{1-x}N$ barrier of $x = 0.08$, $x = 0.12$, and $x = 0.16$.

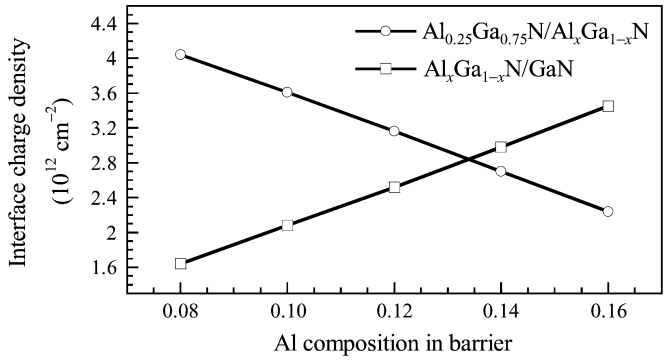

Fig. 8. Theoretically calculated interface charge densities at the $Al_xGa_{1-x}N/GaN$ and $Al_{0.25}Ga_{0.75}N/Al_xGa_{1-x}N$ interfaces as a function of the aluminum composition in barrier layer.

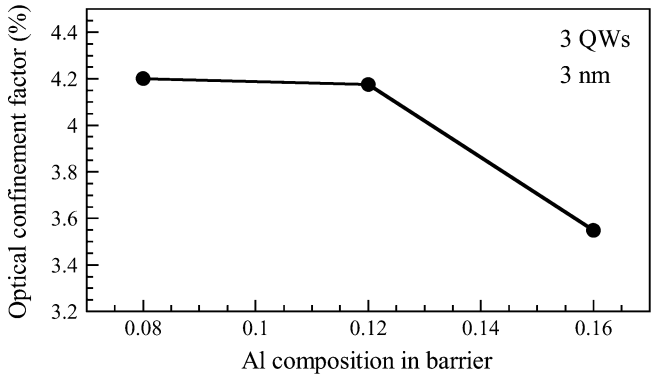

Fig. 9. Quantum-well optical confinement factor versus quantum-barrier aluminum composition when the number of quantum well is three and the quantum-well thickness is 3 nm.

the $Al_xGa_{1-x}N/GaN$ (i.e., the interface between barrier layer and quantum well) and $Al_{0.25}Ga_{0.75}N/Al_xGa_{1-x}N$ (i.e., the interface between electronic blocking layer and barrier layer) interfaces as a function of the aluminum composition in barrier layer. The interface charge densities at the interface between $Al_{0.25}Ga_{0.75}N$ electronic blocking layer and $Al_xGa_{1-t}xN$ barrier layer decrease with increasing aluminum composition in barrier layer. Therefore, the condition of band bending due to the high density of positive polarization charges at the $Al_{0.25}Ga_{0.75}N/Al_xGa_{1-x}N$ interface becomes less evident when the aluminum composition in barrier layer increases, as shown in Fig. 5. On the other hand, the interface charge densities at the interface between $Al_xGa_{1-x}N$ barrier layer and GaN quantum well increase with the barrier aluminum composition, as shown in Fig. 8. In this situation, the built-in polarization causes a deformation of the quantum wells accompanied by a strong electrostatic field, as evident in Fig. 5(c). Therefore, the separation of electrons and holes in the quantum well becomes more obvious with the increasing aluminum composition in barrier layer, as shown in Fig. 6(c). Under this circumstance, the photon emission rate will decrease significantly, which leads to the increase of laser threshold current.

D. Optical Confinement Factor

Except for the effects of electron leakage current, nonuniform electron distribution, and built-in polarization, optical confinement factor is also play an important role for the laser threshold properties. As the aluminum composition in the barrier/confining layer increases, the refractive index decreases simultaneously. Fig. 9 shows the quantum-well optical confinement factor versus quantum-barrier aluminum composition when the number of quantum well is three and the quantum-well thickness is 3 nm. The optical confinement factor decreases with the increasing aluminum composition in barrier layer due to the smaller difference of refractive index between confining layer and cladding layer. For the laser diode with $x = 0.08$, the optical wave intensity is mostly confined within the confining layers. On the contrary, the optical wave intensity is spread into cladding layers as the barrier aluminum composition is 0.16, which leads to the lower optical confinement factor. Although the gain increases with barrier aluminum composition because of the enhanced carrier confinement, the change in confinement factor will decrease the modal gain provided by the laser structure. Therefore, the lower optical confinement factor is also an important role which results in the larger threshold current when the aluminum composition in barrier/confining layer increases.

E. Thickness of the Quantum Well

After investigating the internal physical mechanisms of the GaN/AlGaN laser diodes with different quantum-well numbers and quantum-barrier aluminum compositions, we will further study the effect of quantum-well thickness on laser diode performance. The most nitride-based light-emitting devices are grown by employing relatively thin quantum wells due to the quantum confined Stark effect (QCSE) in the GaN-based quantum wells. The effect is induced by spontaneous and piezoelectric polarization, as discussed in section C. From the view point of the quantum-well structures, the radiative recombination rate is larger with decreasing quantum-well thickness due to the increasing electron-hole wave function overlap [50], [51]. Although the enhanced wave function overlap gives higher material gain for the laser diodes, the thinner quantum well will decrease the optical confinement factor. Fig. 10 shows the threshold current values of the laser diodes with different barrier aluminum compositions when the number of quantum wells varies from one to five. The quantum-well thickness is changed from 3 to 2 nm. In Fig. 10, it is found that the variation of the threshold current values of the laser diodes with 2-nm quantum wells has similar trend as compared with that of the laser diodes with 3-nm quantum wells. This result means that the competition of the above-mentioned physical mechanisms still dominates the threshold properties. Furthermore, it is noteworthy that the threshold current values of the 2-nm quantum-well laser diodes is larger than that of the 3-nm quantum-well laser diodes. This reason can be found from Fig. 11, which shows the quantum-well optical confinement factor versus quantum-barrier aluminum composition for the 2-nm GaN/AlGaN triple-quantum-well laser diodes. By comparing Fig. 11 and Fig. 9, the lower optical confinement factor is one of the most important factors which results in the higher threshold current of the laser diodes with 2-nm quantum wells. Besides, the thinner quantum well will induce larger electron leakage current, which is observed in our calculation.

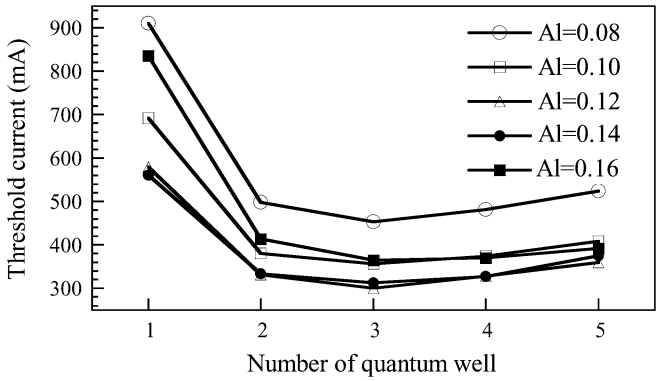

Fig. 10. Threshold current values of laser diodes with different barrier aluminum composition when the number of quantum well varies form one to five. The quantum-well thickness is 2 nm.

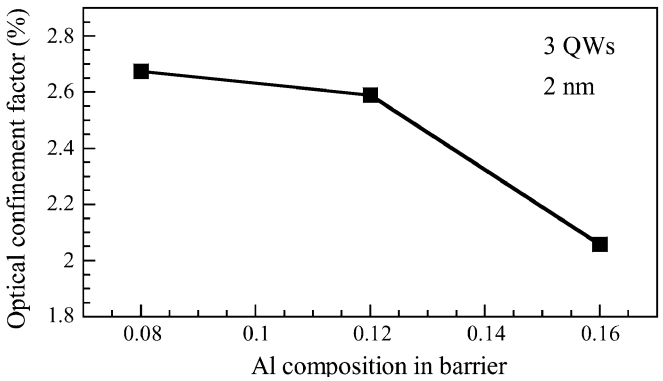

Fig. 11. Quantum-well optical confinement factor versus quantum-barrier aluminum composition when the number of quantum well is three and the quantum-well thickness is 2 nm.

As for the laser diodes with larger quantum-well thickness than 3 nm, not presented here, the higher threshold current values are also found in our simulation due to the increase of electron-hole wave function separation. Therefore, 3-nm quantum-well thickness is optimal to balance the advantages of a large confinement factor against the disadvantages of QCSE for the ultraviolet laser diodes [16]. This quantum-well thickness is mostly employed in the nitride-based ultraviolet laser diodes [7], [13], [14], [16].

IV. Conclusion

We have done the theoretical simulation to investigate the effects of quantum-well number, quantum-barrier aluminum composition, and quantum-well thickness on the GaN/AlGaN multiple-quantum-well laser performance. The relations between the electron leakage currents and the active region structures, for different numbers of quantum well and aluminum compositions in the barrier/confining layers, are discussed and analyzed. The simulation results indicate that, among the active layer structures under study, lower threshold current can be achieved when the number of quantum wells is two or three and the aluminum composition in barrier/confining layer is about 10%–12%. Five different effects cause this result. First, the severe electron leakage current is observed due to the lower barrier aluminum composition and fewer number of quantum wells. Second, the obvious nonuniform distribution of electron carriers is found due to the higher barrier aluminum composition and the more number of quantum wells. Third, the higher density of positive polarization charges at the interface between the $Al_xGa_{1-x}N$ barrier layer and the $Al_{0.25}Ga_{0.75}N$ electronic blocking layer with decreasing barrier aluminum composition is also another important factor which enhances the electron leakage current. Fourth, the interface charge density at the interface between $Al_xGa_{1-x}N$ barrier layer and GaN quantum well increases with the barrier aluminum composition, which lowers the photon emission rate. Fifth, the optical confinement factor decreases with the increasing aluminum composition in barrier layer, which leads to the larger threshold current. Therefore, the GaN/AlGaN laser diode with an active layer of two or three quantum wells and $x = 0.10 \sim 0.12$ in the $Al_xGa_{1-x}N$ barrier/confining layer has found to be the optimized active layer structure due to the competition of these five internal physical mechanisms. Furthermore, the simulation results also indicate that the optimal quantum-well thickness is about 3 nm due to the balance of the advantages of a large confinement factor against the disadvantages of significant QCSE.

References

[1] E. F. Schubert and J. K. Kim, "Solid-state light sources getting smart," *Science*, vol. 308, pp. 1274–1278, 2005.

[2] S. Nakamura and G. Fasol, *The Blue Laser Diode.*. Berlin, Germany: Springer-Verlag, 1997.

[3] D. A. Steigerwald, J. C. Bhat, D. Collins, R. M. Fletcher, M. O. Holcomb, M. J. Ludowise, P. S. Martin, and S. L. Rudaz, "Illumination with solid state lighting technology," *IEEE J. Sel. Topics Quant. Electron.*, vol. 8, no. 2, pp. 310–320, Mar./Apr. 2002.

[4] S. Nakamura, M. Senoh, and T. Mukai, "Highly p-typed Mg-doped GaN films grown with GaN buffer layers," *Jpn. J. Appl. Phys.*, vol. 30, pp. L1708–L1711, 1991.

[5] S. Nakamura, N. Iwasa, M. Senoh, and T. Mukai, "Hole compensation mechanism of p-type GaN films," *Jpn. J. Appl. Phys.*, vol. 31, pp. 1258–1266, 1992.

[6] M. A. Khan, M. Shatalov, H. P. Maruska, H. M. Wang, and E. Kuokstis, "III-nitride UV devices," *Jpn. J. Appl. Phys.*, vol. 44, pp. 7191–7206, 2005.

[7] S. Kamiyama, K. Iida, T. Kawashima, H. Kasugai, S. Mishima, A. Honshio, Y. Miyake, M. Iwaya, H. Amano, and I. Akasaki, "UV laser diode with 350.9-nm-lasing wavelength grown by hetero-epitaxial-lateral overgrowth technology," *IEEE J. Sel. Topics Quant. Electron.*, vol. 11, no. 5, pp. 1069–1073, Sep./Oct. 2005.

[8] J. Li, T. N. Oder, M. L. Nakarmi, J. Y. Lin, and H. X. Jiang, "Optical and electrical properties of Mg-doped p-type $Al_xGa_{1-x}N$," *Appl. Phys. Lett.*, vol. 80, pp. 1210–1212, 2002.

[9] G. Franssen, S. Grzanka, R. Czernecki, T. Suski, L. Marona, T. Riemann, J. Christen, H. Teisseyre, P. Valvin, P. Lefebvre, P. Perlin, M. Leszczyñski, and I. Grzegory, "Efficient radiative recombination and potential profile fluctuations in low-dislocation InGaN/GaN multiple quantum wells on bulk GaN substrates," *J. Appl. Phys.*, vol. 97, p. 103507, 2005.

[10] S. Masui, Y. Matsuyama, T. Yanamoto, T. Kozaki, S. Nagahama, and T. Mukai, "365 nm ultraviolet laser diodes composed of quaternary AlInGaN alloy," *Jpn. J. Appl. Phys.*, vol. 42, pp. L1318–L1320, 2003.

[11] M. Kneissl, D. W. Treat, M. Teepe, N. Miyashita, and N. M. Johnson, "Ultraviolet AlGaN multiple-quantum-well laser diodes," *Appl. Phys. Lett.*, vol. 82, pp. 4441–4443, 2003.

[12] J. Edmond, A. Abare, M. Bergman, J. Bharathan, K. L. Bunker, D. Emerson, K. Haberern, J. Ibbetson, M. Leung, P. Russel, and D. Slater, "High efficiency GaN-based LEDs and lasers on SiC," *J. Cryst. Growth*, vol. 272, pp. 242–250, 2004.

[13] K. Iida, T. Kawashima, A. Miyazaki, H. Kasugai, S. Mishima, A. Honshio, Y. Miyake, M. Iwaya, S. Kamiyama, H. Amano, and I. Akasaki, "350.9 nm UV laser diode grown on low-dislocation-density AlGaN," *Jpn. J. Appl. Phys.*, vol. 43, pp. L499–L500, 2004.

[14] K. Iida, T. Kawashima, A. Miyazaki, H. Kasugai, S. Mishima, A. Honshio, Y. Miyake, M. Iwaya, S. Kamiyama, H. Amano, and I. Akasaki, "Laser diode of 350.9 nm wavelength grown on sapphire substrate by MOVPE," *J. Cryst. Growth*, vol. 272, pp. 270–273, 2004.
[15] LASTIP Version 2005.11. Burnaby, BC, Canada, 2005, Crosslight Software.
[16] W. W. Chow, M. Kneissl, J. E. Northrup, and N. M. Johnson, "Influence of quantum-well-barrier composition on gain and threshold current in AlGaN lasers," *Appl. Phys. Lett.*, vol. 90, p. 101116, 2007.
[17] Y.-K. Kuo and Y.-A. Chang, "Effects of electronic current overflow and inhomogeneous carrier distribution on InGaN quantum-well laser performance," *IEEE J. Quant. Electron.*, vol. 40, no. 5, pp. 437–444, May 2004.
[18] S. L. Chuang and C. S. Chang, "k·p method for strained wurtzite semiconductors," *Phys. Rev. B*, vol. 54, pp. 2491–2504, 1996.
[19] S. L. Chuang and C. S. Chang, "Effective-mass Hamiltonian for strained wurtzite GaN and analytical solutions," *Appl. Phys. Lett.*, vol. 68, pp. 1657–1659, 1996.
[20] I. Vurgaftman and J. R. Meyer, "Band parameters for nitrogen-containing semiconductors," *J. Appl. Phys.*, vol. 94, pp. 3675–3691, 2003.
[21] S. L. Chuang, "Optical gain of strained wurtzite GaN quantum-well lasers," *IEEE J. Quant. Electron.*, vol. 32, no. 10, pp. 1791–1799, Oct. 1996.
[22] Y. C. Yeo, T. C. Chong, M.-F. Li, and W. J. Fan, "Electronic band structures and optical gain spectra of strained wurtzite GaN-$Al_xGa_{1-x}N$ quantum-well lasers," *IEEE J. Quant. Electron.*, vol. 34, no. 3, pp. 526–534, Mar. 1998.
[23] Y. C. Yeo, T. C. Chong, M. F. Li, and W. J. Fan, "Analysis of optical gain and threshold current density of wurtzite InGaN/GaN/AlGaN quantum well lasers," *J. Appl. Phys.*, vol. 84, pp. 1813–1819, 1998.
[24] C. G. Van de Walle and J. Neugebauer, "Universal alignment of hydrogen levels in semiconductors, insulators and solutions," *Nature*, vol. 423, pp. 626–628, 2003.
[25] V. Fiorentini, F. Bernardini, and O. Ambacher, "Evidence for nonlinear macroscopic polarization in III-V nitride alloy heterostructures," *Appl. Phys. Lett.*, vol. 80, pp. 1204–1206, 2002.
[26] J. P. Ibbetson, P. T. Fini, K. D. Ness, S. P. DenBaars, J. S. Speck, and U. K. Mishra, "Polarization effects, surface states, and the source of electrons in AlGaN/GaN heterostructure field effect transistors," *Appl. Phys. Lett.*, vol. 77, pp. 250–252, 2000.
[27] S. F. Chichibu, A. C. Abare, M. S. Minsky, S. Keller, S. B. Fleischer, J. E. Bowers, E. Hu, U. K. Mishra, L. A. Coldren, S. P. DenBaars, and T. Sota, "Effective band gap inhomogeneity and piezoelectric field in InGaN/GaN multiquantum well structures," *Appl. Phys. Lett.*, vol. 73, pp. 2006–2008, 1998.
[28] H. Zhang, E. J. Miller, E. T. Yu, C. Poblenz, and J. S. Speck, "Measurement of polarization charge and conduction-band offset at In $_xGa_{1-x}$N/GaN heterojunction interfaces," *Appl. Phys. Lett.*, vol. 84, pp. 4644–4646, 2004.
[29] F. Renner, P. Kiesel, G. H. Dõhler, M. Kneissl, C. G. Van de Walle, and N. M. Johnson, "Quantitative analysis of the polarization fields and absorption changes in InGaN/GaN quantum wells with electroabsorption spectroscopy," *Appl. Phys. Lett.*, vol. 81, pp. 490–492, 2002.
[30] C. M. Caughey and R. E. Thomas, "Carrier mobilities in silicon empirically related to doping and field," *Proc. IEEE*, vol. 55, no. 12, pp. 2192–2193, Dec. 1967.
[31] T. T. Mnatsakanov, M. E. Levinshtein, L. I. Pomortseva, S. N. Yurkov, G. S. Simin, and M. A. Khan, "Carrier mobility model for GaN," *Solid State Electron.*, vol. 47, pp. 111–115, 2003.
[32] F. Schwierz, "An electron mobility model for wurtzite GaN," *Solid State Electron.*, vol. 49, pp. 889–895, 2005.
[33] M. Farahmand, C. Garetto, E. Bellotti, K. F. Brennan, M. Goano, E. Ghillino, G. Ghione, J. D. Albrecht, and P. P. Ruden, "Monte Carlo simulation of electron transport in the III-nitride wurtzite phase materials system: binaries and ternaries," *IEEE Trans. Electron Devices*, vol. 48, no. 3, pp. 535–542, Mar. 2001.
[34] M. F. Huang and T. H. Lu, "Optimization of the active-layer structure for the deep-UV AlGaN light-emitting diodes," *IEEE J. Quant. Electron.*, vol. 42, no. 8, pp. 820–826, Aug. 2006.
[35] Y. K. Kuo, S. H. Yen, and J. R. Chen, "Ultraviolet Light-Emitting Diodes," in *Nitride Semiconductor Devices: Principles and Simulation*. Berlin, Germany: Wiley-VCH Verlag, 2007.
[36] J. Piprek, T. Katona, S. P. DenBaars, and S. Li, "3D simulation and analysis of AlGaN/GaN ultraviolet light emitting diodes," *Proc. SPIE*, vol. 5366, pp. 127–136, 2004.
[37] B. Romero, J. Arias, I. Esquivias, and M. Cada, "Simple model for calculating the ratio of the carrier capture and escape times in quantum-well lasers," *Appl. Phys. Lett.*, vol. 76, pp. 1504–1506, 2000.
[38] S. Adachi, *Physical Properties of III-V Semiconductor Compounds*. New York: Wiley, 1992.
[39] T. Peng and J. Piprek, "Refractive index of AlGaInN alloys," *Electron. Lett.*, vol. 32, pp. 2285–2286, 1996.
[40] G. M. Laws, E. C. Larkins, I. Harrison, C. Molloy, and D. Somerford, "Improved refractive index formulas for the $Al_xGa_{1-x}N$ and In $_yGa_{1-y}$N alloys," *J. Appl. Phys.*, vol. 89, pp. 1108–1110, 2001.
[41] J. Piprek, *Semiconductor Optoelectronic Devices: Introduction to Physics and Simulation*. San Diego, CA: Academic, 2003.
[42] J. Piprek and S. Li, "GaN-based Light-Emitting Diodes," in *Optoelectronic Devices: Advanced Simulation and Analysis*. New York: Springer Verlag, 2005.
[43] Y. K. Kuo, S. H. Yen, and J. R. Chen, "Ultraviolet light-emitting diodes," in *Nitride Semiconductor Devices: Principles and Simulation*. Berlin, Germany: Wiley-VCH Verlag, 2007.
[44] K. Domen, R. Soejima, A. Kuramata, and T. Tanahashi, "Electron overflow to the AlGaN p-cladding layer in InGaN/GaN/AlGaN MQW laser diodes," *MRS Internet J. Nitride Semicond. Res.*, vol. 3, no. 2, 1998.
[45] J. Y. Chang and Y. K. Kuo, "Simulation of blue InGaN quantum-well lasers," *J. Appl. Phys.*, vol. 93, pp. 4992–4998, 2003.
[46] J. Piprek, R. Farrell, S. DenBaars, and S. Nakamura, "Effects of built-in polarization on InGaN-GaN vertical-cavity surface-emitting lasers," *IEEE Photon. Technol. Lett.*, vol. 18, no. 1, pp. 7–9, Jan. 2006.
[47] S.-N. Lee, S. Y. Cho, H. Y. Ryu, J. K. Son, H. S. Paek, T. Sakong, T. Jang, K. K. Choi, K. H. Ha, M. H. Yang, O. H. Nam, Y. Park, and E. Yoon, "High-power GaN-based blue-violet laser diodes with AlGaN/GaN multiquantum barriers," *Appl. Phys. Lett.*, vol. 88, p. 111101, 2006.
[48] J. Piprek, P. Abraham, and J. E. Bowers, "Carrier nonuniformity effects on the internal efficiency of multiquantum-well lasers," *Appl. Phys. Lett.*, vol. 74, pp. 489–491, 1999.
[49] J. D. Heber, C. Gmachl, H. M. Ng, and A. Y. Cho, "Comparative study of ultrafast intersubband electron scattering times at $\sim 1.55\ \mu$m wavelength in GaN/AlGaN heterostructures," *Appl. Phys. Lett.*, vol. 81, pp. 1237–1239, 2002.
[50] C.-K. Sun, S. Keller, T.-L. Chiu, G. Wang, M. S. Minsky, J. E. Bowers, and S. P. Denbaars, "Well-width dependent studies of InGaN-GaN single-quantum wells using time-resolved photoluminescence techniques," *IEEE J. Sel. Topics Quant. Electron.*, vol. 3, no. 3, pp. 731–737, Jun. 1997.
[51] E. Berkowicz, D. Gershoni, G. Bahir, E. Lakin, D. Shilo, E. Zolotoyabko, A. C. Abare, S. P. Denbaars, and L. A. Coldren, "Measured and calculated radiative lifetime and optical absorption of In $_xGa_{1-x}$N/GaN quantum structures," *Phys. Rev. B*, vol. 61, pp. 10994–11008, 2000.

Jun-Rong Chen was born in Taichung, Taiwan, R.O.C., on October 23, 1980. He received the B.S. degree in physics from the National Changhua University of Education (NCUE), Changhua, Taiwan, in 2004, and the M.S. degree in optoelectronics from the Institute of Photonics, NCUE, Taiwan, in 2006. He is currently working toward the Ph.D. degree in the Department of Photonics and Institute of Electro-Optical Engineering, National Chiao Tung University (NCTU), Hsinchu, Taiwan.

He joined the Semiconductor Laser Technology Laboratory at NCTU in 2006, where he was engaged in research on III-V semiconductor materials for light-emitting diodes and semiconductor lasers under the instruction of Prof. T.-C. Lu, Prof. H.-C. Kuo, and Prof. S.-C. Wang. His recent research interests include III-nitride semiconductor lasers, epitaxial growth of III-nitride materials, and numerical simulation of III-V optoelectronic devices.

Tsung-Shine Ko was born in Tainan, Taiwan, R.O.C., in 1978. He received the B.S. degree in physics from the National Changhua University, Changhua, Taiwan, in 2001, and the M.S. degree in atomic science from the National Tsing Hau University, Hsinchu, Taiwan, in 2004. He is currently working toward the Ph.D. degree in the Department of Photonics and Institute of Electro-Optical Engineering, National Chiao Tung University (NCTU), Hsinchu, Taiwan.

He was engaged in research on design of masks for extreme ultraviolet (EUV), the synthesis of gold nanoprticles and the growth of Si/Ge nanostructures under the instruction of Dr. J. Shieh, Prof. H. L. Chen, and Prof. T. C. Chu. His recent research interests include fabrication of nanostructure oxide materials and epitaxial growth of nonpolar GaN based materials under the instruction of Prof. T.-C. Lu, Prof. H.-C. Kuo, and Prof. S.-C. Wang. He is going to join Prof. J. Han's group at Yale University, New Haven, CT, during 2008–2009 and mainly engage in further topics related to nitride-based materials and devices.

Po-Yuan Su was born in Kaohsiung, Taiwan, R.O.C., on December 8, 1983. He received the B.S. degree in engineering science from the National Cheng Kung University (NCKU), Tainan, Taiwan, in 2006. He is currently working toward the M.S. degree in the Department of Photonics and Institute of Electro-Optical Engineering, National Chiao Tung University (NCTU), Hsinchu, Taiwan.

He joined the Semiconductor Laser Laboratory, NCTU, in 2006, where he was engaged in simulation on III-nitride semiconductor devices including light-emitting diodes and semiconductor laser diodes under the instruction of Prof. T.-C. Lu, Prof. H.-C. Kuo, and Prof. S.-C. Wang. His recent research interests in numerical simulation of III-nitride optoelectronic devices.

Tien-Chang Lu (M'07) received the B.S. degree in electrical engineering from the National Taiwan University, Taipei, Taiwan, R.O.C., in 1995, the M.S. degree in electrical engineering from the University of Southern California, Los Angeles, in 1998, and the Ph.D. in electrical engineering and computer science from the National Chiao Tung University, Hsinchu, Taiwan, in 2004.

He was with the Union Optronics Corporation as a Manager of Epitaxy Department in 2004. Since Auguest 2005, he has been with the National Chiao Tung University as a member of the faculty in the Department of Photonics. His research work included the design, epitaxial growth, process, and characterization of optoelectronic devices, such as Fabry–Perot-type semiconductor lasers, vertical-cavity surface-emitting lasers, resonant-cavity light-emitting diodes (LEDs), wafer-fused flip-chip LEDs, solar cells, etc. He has been engaged in the low-pressure MOCVD epitaxial technique associated with various material systems including InGaAlAs, InGaAsP, AlGaAs, InGaAlP, and InGaAlN, as well as the corresponding process skills. He is also interested in the structure design and simulations for optoelectronic devices using computer-aided software.

Hao-Chung Kuo (S'98–M'99–SM'06), received the B.S. degree in physics from the National Taiwan University, Taipei, Taiwan, R.O.C., in 1990, the M.S. degree in electrical and computer engineering from Rutgers University, Camden, NJ, in 1995, and the Ph.D. degree in electrical and computer engineering from the University of Illinois at Urbana-Champaign, Urbana, in 1999.

He has an extensive professional career both in research and industrial research institutions, which includes as follows: Research Consultant with Lucent Technologies, Bell Labs, Holmdel, NJ (from 1995 to 1997); R&D Engineer with the Fiber-Optics Division, Agilent Technologies (from 1999 to 2001); and R&D Manager with LuxNet Corporation (from 2001 to 2002). Since September 2002, he has been with the National Chiao Tung University, Hsinchu, Taiwan, as a member of the faculty at the Institute of Electro-Optical Engineering. He has authored or coauthored over 60 publications. His current research interests include the epitaxy, design, fabrication, and measurement of high-speed InP- and GaAs-based vertical-cavity surface-emitting lasers, as well as GaN-based lighting-emitting devices and nanostructures.

Yen-Kuang Kuo was born in Chia-Yi, Taiwan, R.O.C., on July 19, 1959. He received the B.S. degree in electrophysics from the National Chiao-Tung University, Hsin Chu, Taiwan, in 1982, the M.S. degree in electrical engineering from the National Taiwan University, Taipei, Taiwan, in 1984, and the Ph.D. degree in electrical engineering from the University of Southern California (USC), Los Angeles, in 1994.

From 1984 to 1991, he was with the Aeronautical Research Laboratory, Chung Shan Institute of Science and Technology, Taichung, Taiwan. He was a Postdoctoral Research Fellow with the Center for Laser Studies, USC, from 1994 to 1995, where he was engaged in research on passive Q-switching with solid-state saturable absorbers. From 1995 to 1997, he was with the Aerospace Industrial Development Corporation, Taichung, Taiwan. In 1997, he joined the faculty of the Department of Physics, National Changhua University of Education, Changhua, Taiwan, where he is a Professor with the Department of Physics and Institute of Photonics and Head of the Laboratory of Lasers and Optical Semiconductors. His recent research interests include passive Q-switching with solid-state saturable absorbers and semiconductor materials for light-emitting diodes, organic light-emitting diodes, and semiconductor lasers.

Shing-Chung Wang (M'79–SM'03) received the B.S. degree in electrical engineering from the National Taiwan University, Taipei, Taiwan, R.O.C., in 1957, the M.S. degree in electrical engineering from the National Tohoku University, Sendai, Japan, in 1965, and the Ph.D. degree in electrical engineering from the Stanford University, Stanford, CA, in 1971.

He has an extensive professional career both in academic and industrial research institutions, which includes the following: member of the faculty at the National Chiao Tung University, Hsinchu, Taiwan (from 1965 to 1967), Research Associate with Stanford University (from 1971 to 1974), Senior Research Scientist with Xerox Corporation (from 1974 to 1985), and Consulting Scientist with Lockheed-Martin Palo Alto Research Laboratories (from 1985 to 1995). Since 1995, he has been a member of the faculty at the Institute of Electro-Optical Engineering, National Chiao Tung University. He has authored or coauthored over 160 publications. His current research interests include semiconductor lasers, vertical-cavity surface-emitting lasers, blue and UV lasers, quantum-confined optoelectronic structures, optoelectronic materials, diode-pumped lasers, and semiconductor-laser applications.

Prof. Wang is a Fellow of the Optical Society of America and the recipient of the Outstanding Scholar Award from the Foundation for the Advancement of Outstanding Scholarship.